

THE OFFICIAL MAGAZINE OF THE OCEANOGRAPHY SOCIETY

Oceanography

CITATION

Monaldo, F.M., C.R. Jackson, and W.G. Pichel. 2013. Seasat to RADARSAT-2: Research to operations. *Oceanography* 26(2):34–45, <http://dx.doi.org/10.5670/oceanog.2013.29>.

DOI

<http://dx.doi.org/10.5670/oceanog.2013.29>

COPYRIGHT

This article has been published in *Oceanography*, Volume 26, Number 2, a quarterly journal of The Oceanography Society. Copyright 2013 by The Oceanography Society. All rights reserved.

USAGE

Permission is granted to copy this article for use in teaching and research. Republication, systematic reproduction, or collective redistribution of any portion of this article by photocopy machine, reposting, or other means is permitted only with the approval of The Oceanography Society. Send all correspondence to: info@tos.org or The Oceanography Society, PO Box 1931, Rockville, MD 20849-1931, USA.

SEASAT TO RADARSAT-2

RESEARCH TO
OPERATIONS

BY FRANK M. MONALDO,
CHRISTOPHER R. JACKSON,
AND WILLIAM G. PICHEL

ABSTRACT. In 2013, the National Oceanic and Atmospheric Administration (NOAA) brought to operations a synthetic aperture radar (SAR)-derived subkilometer resolution wind speed product. This transition from research to operations comes 35 years after the 1978 launch of the US Seasat satellite, which demonstrated that radar backscatter from active microwave instruments in orbit can provide detailed information about ocean surface waves, winds, and sea surface height. NOAA's initial source of data for operational SAR winds is RADARSAT-2, which was launched in 2007 by the Canadian Space Agency. In this paper, we discuss the history of our understanding of the relationship between microwave measurements, particularly SAR measurements, and wind speed, and how a spaceborne instrument first designed to measure ocean waves is now routinely used to derive wind speeds.

INTRODUCTION: A SHORT HISTORY

Measurement of the ocean surface using microwaves began with sensors deployed far closer to Earth than orbit. Radar interference from the ocean surface affected military operations, especially during World War II when radar technology was emerging. Consequently, there was a strong interest in understanding such effects. Rice (1951) and Kerr (1951) pursued the notion that backscattered power from the surface increased when the wavelength of the radar matched the ocean surface wavelength, analogous to Bragg resonance measured from scattering off of crystal structures (Bragg, 1913). As radar frequencies increased and wavelengths decreased, this same phenomenon was observed in microwave radar (> 1 GHz

frequency) regimes (Wright, 1966, 1968; Valenzuela, 1968; Phillips, 1988; Plant, 1990). Bragg scattering would prove to be the key to understanding how to measure winds over the ocean from space.

The first spaceborne active radar for Earth remote sensing was RADSCAT, which flew aboard Skylab (Moore, 1974). The combined 13.9 GHz radiometer and scatterometer measured the ocean at four polarizations (HH, VV, VH, and HV; see Ager, 2013, in this issue for a discussion of the polarizations) and at nadir incident angles of 0°, 15°, 30°, 40°, and 50°. It demonstrated the fundamental ability to make both wind and wave measurements. Given the success of RADSCAT and the less risk-adverse nature of the times, Seasat followed rapidly in 1978.

Seasat carried a suite of new sensors designed to measure various aspects of the ocean surface. There was a radar altimeter that could measure sea surface height, wind speed, and significant wave height; a microwave radiometer for (among other things) wind speed measurements; an active microwave scatterometer for wind speed; and an

L-band synthetic aperture radar (SAR; Jordan, 1980) for ocean surface wave spectra. In addition, the Seasat SAR imagery showed subkilometer-resolution features associated with wind field variability (Vesecky and Stewart, 1982; Fu and Holt, 1982).

The Seasat Ku-band scatterometer (SASS, for Seasat-A Scatterometer System) was equipped with four stick antennas and operated at 14.6 GHz with dual-polarization that measured winds at 100 km resolution. The scatterometer served as a prototype for a generation of spaceborne scatterometers, from the Active Microwave Instrument (AMI; Attema, 1991), to the National Aeronautics and Space Administration (NASA) Scatterometer (NSCAT; Naderi et al., 1991), to SeaWinds (Spencer et al., 1997), to the Advanced Scatterometer (ASCAT; Figa-Saldana et al., 2002), and others. These scatterometer measurements are an important input to global weather models.

At a variety of microwave frequencies, off-nadir measurements of normalized radar cross section (NRCS) follow a functional relationship of the form

$$\sigma^0 = A(f, p, \theta) U^{\gamma(f, p, \theta)} [1 + B(f, p, \theta) \cos \varphi + C(f, p, \theta) \cos 2\varphi], \quad (1)$$

where σ^0 is the normalized radar cross section as a function of wind speed, U , and the relative angle between the wind direction and the radar look direction, φ . The coefficients A , B , C , and γ are dependent upon frequency, f , polarization, p , and incident angle, θ . Over the years, there have been many permutations of this functional form, but Equation 1 retains saliency as a notional description.

OPPOSITE PAGE IMAGE: Mosaic of RADARSAT-2 synthetic aperture radar (SAR) images from March 18 and 19, 2013, over southwestern Alaska and the eastern Bering Sea produced by the National Oceanographic and Atmospheric Administration's (NOAA's) operational SAR winds retrieval system for the National Ice Center. In addition to wind speed over open water, strong sea ice returns are apparent in the images.

The key feature of Equation 1 is that for a given a wind speed and direction, it is possible to compute an associated σ^0 . The inverse, however, is not true. A single ocean surface NRCS measurement can correspond to a large num-

ber of wind field continuity and/or consistency with numerical wind model predictions.

The L-band (1.274 GHz) Seasat SAR was designed not for wind but rather to make 25 m resolution NRCS

speed values was still to find some way to invert Equation 1 using a single σ^0 measurement. If the wind direction is known a priori, then Equation 1 can be inverted. SAR's high resolution offered a possibility for inferring wind direction. A number of investigators noticed linear streaks or features on the scale of 1 to 3 km in the SAR image that were aligned with the wind direction, perhaps associated with roll vortices in the marine boundary layer (Brown, 1980, 1986). Thus, SAR imagery itself provides a clue, albeit with a 180° ambiguity, to wind direction.

In a seminal paper, Gerling (1986) exploited this for Seasat SAR data. Gerling broke a strip of SAR imagery off the east coast of the United States (pass 1339) into eighteen 25.6 × 25.6 km frames averaged to 100 m resolution. He then computed the two-dimensional discrete Fourier transform of each frame, resolving the spatial frequency variations between 25.6 km and 200 m. Gerling (1986) was able to use this low-frequency spatial spectral information to infer the direction of the wind rows and hence the wind direction. These directions were consistent with coincident wind direction measurements from the Seasat scatterometer.

Later, others exploited this technique or similar ones to estimate wind direction using ERS-1 (Vachon and Dobson, 1996; Wackerman et al., 1996; Horstmann, 1997; Fetterer et al., 1998; Lehner et al., 1998), RADARSAT-1 (Horstmann et al., 2000, 2002; Wackerman, 2000; Wackerman et al., 2003), and Envisat (Horstmann et al., 2003) SAR data, and then used the estimated directions to compute wind speed.

Sometimes linear features in SAR images are not available for wind

“ IN THIS PAPER, WE DISCUSS THE HISTORY OF OUR UNDERSTANDING OF THE RELATIONSHIP BETWEEN MICROWAVE MEASUREMENTS, PARTICULARLY SAR MEASUREMENTS, AND WIND SPEED, AND HOW A SPACEBORNE INSTRUMENT FIRST DESIGNED TO MEASURE OCEAN WAVES IS NOW ROUTINELY USED TO DERIVE WIND SPEEDS. ”

ber of wind speed and direction pairs. This important characteristic was well understood by those who designed SASS (Boggs, 1982). As the multi-antenna scatterometer flew, it measured different σ^0 values from the same areas of the ocean at different polarizations, incident angles, and aspect angles with respect to the wind, such that a set of equations of the form of Equation 1 were obtained. Given these σ^0 measurements, it was possible to produce a set of up to four wind speed and direction pairs consistent with the measurements. Usually, the actual wind speed vector could be resolved into a single vector on

measurements over a 100 km swath for the purpose of ocean surface wave height spectra measurements. Unlike the scatterometer, for each position on the surface, there was only a single NRCS measurement, at a single incident angle, at a single frequency, with a single polarization, and with a single aspect angle with respect to the local wind direction. Nonetheless, Weissman et al. (1979), Beal (1980), Beal et al. (1983), and Jones et al. (1981) observed a correspondence between the L-band Seasat SAR image intensity and Seasat scatterometer wind speed.

The key to computing SAR wind

Frank M. Monaldo (frank.monaldo@jhuapl.edu) is Principal Staff Physicist, Johns Hopkins University Applied Physics Laboratory, Laurel, MD, USA. **Christopher R. Jackson** (goa@internalwaveatlas.com) is Chief Scientist, Global Ocean Associates, supporting the National Oceanic and Atmospheric Administration/National Environmental Satellite, Data, and Information Service (NOAA/NESDIS) at College Park, MD, USA. **William G. Pichel** is a research scientist with NOAA/NESDIS, College Park, MD, USA.

direction estimates, so investigators have also pursued an alternative approach. It is also possible to use wind direction information from numerical weather models to initiate SAR wind speed retrieval. Model wind directions may not be able to show very high-resolution changes in wind direction, but they do have the benefit of always providing a wind direction field that is reasonable, dynamically in balance, and unencumbered with a 180° ambiguity. Using model data from the Navy Operational Global Atmospheric Prediction System (NOGAPS) and data from the RADARSAT-1 SAR satellite, wind speed retrievals were shown to agree with buoy and QuikSCAT SeaWinds scatterometer measurements with standard deviations of less than 2 m s⁻¹ (Thompson and Beal, 2000; Monaldo et al., 2001, 2003, 2004; Thompson et al., 2001).

We note that the increase in wind speed error with increasing wind speed is a consequence of the fact that the wind speed to σ^0 relationship begins to saturate at higher wind speeds. A fixed change in σ^0 requires a larger change in wind speed. A fixed NRCS measurement error will correspond to larger wind speed errors. Horstmann et al. (2003, 2011) discuss the wind speed error dependence on SAR geometry and wind speed.

TOWARD OPERATIONS

Following Seasat, there has been a steady increase in the number of SAR satellites (Table 1), accompanied by an increase in resolution, polarization diversity, and swath coverage area. L-band has generally found its way into land applications. C-band is best understood for ocean scattering and is, therefore, the preferred

choice for SAR wind speed retrieval. X-band is useful for achieving very high resolutions with modest size antennas. The full exploitation of X-band for SAR wind retrieval is just beginning.

Although the first Seasat SAR wind speed retrievals were at L-band (Gerling, 1986), from 1991 to the present there has always been a spaceborne C-band SAR acquiring imagery. Considerable experimental and theoretical efforts have been devoted to understanding and validating the C-band geophysical model function (GMF)—the relationship between wind speed and direction and σ^0 expressed in Equation 1. Proposed GMFs include CMOD4 (Attema, 1986; Stoffelen and Anderson, 1993, 1997a,b), CMOD IFR2 (IFREMER, 1996), CMOD5 (Hersbach, 2003), and CMOD5n (Hersbach, 2008).

These model functions were designed for VV-polarization to suit the ERS-1/2 and later Envisat SARs.

RADARSAT-1's primary mission was sea ice identification and location for which HH-polarization was most apt. To use RADARSAT-1 for wind speed retrieval required the development of an HH-polarization model function. To meet this challenge, Thompson et al. (1999 and 2001) proposed a polarization ratio that mapped VV-polarization radar cross section in HH-polarization cross section using the equation

$$\sigma_{HH}^0 = \sigma_{VV}^0 \frac{(1 + \alpha \tan \theta)^2}{(1 + 2 \tan \theta)^2}, \quad (2)$$

where θ is the incident angle and α is a parameter dependent on the exact nature of the scattering. It has been determined that $\alpha = 0.6$ yields the best comparisons with respect to independent wind estimates for RADARSAT-1 SAR data (Monaldo et al., 2001).

With RADARSAT-1, the US and Canadian governments maintained a data sharing arrangement whereby

Table 1. Summary of free-flying spaceborne SARs (Moreira et al., 2013).

Satellite	Launch	Frequency	Polarization	Resolution
Seasat	1978	L	HH	25 m
ERS-1	1991	C	VV	25 m
JERS-1	1992	L	HH	18 m
ERS-2	1995	C	VV	25 m
RADARSAT-1	1995	C	HH	25–50 m
Envisat	2002	C	VV, HH, HV, VH*	30–1,000 m
ALOS	2006	L	Full-Pol	7–88 m
TerraSAR-X	2007	X	Full-Pol	3 m
RADARSAT-2	2007	C	Full-Pol	3–100 m
COSMO-SkyMed 1-4	2007–2010	X	HH, VV	3 m
TanDEM-X	2010	X	Full-Pol	3 m
ALOS-2	2013	L	Full-Pol	7–88 m
Sentinel-1A	2014	C	HH, VV, VH, HV*	5–20 m

* Dual-polarization ability.

large quantities of imagery (over the Bering, Beaufort, and Chukchi Seas and the Gulf of Alaska) were downlinked and processed at the Alaska Satellite Facility (ASF). This imagery provided the first real opportunity within NOAA to produce SAR-derived winds from large quantities of near real-time imagery on a regular basis. To leverage this opportunity in 1999, the Alaska SAR Demonstration (AKDEMO; Pichel and Clemente-Colón, 2000) was put in place by NOAA's National Environmental Satellite, Data, and Information Service (NESDIS) and Center for Satellite

Applications and Research (STAR) to: (1) validate and test prototype SAR products that respond to critical needs, (2) provide these products in near-real time for trial use by operational agencies, and (3) provide education and training materials to users toward better understanding of SAR imagery and its derived products. The software and protocols developed to produce real-time SAR winds as part of AKDEMO evolved into the Johns Hopkins Applied Physics Laboratory (APL)/NOAA SAR Wind Retrieval System (ANSWRS).

As part of AKDEMO, RADARSAT-1

calibrated σ^0 imagery from ASF were sent to NOAA and processed into wind speed imagery at 500 m resolution using wind directions obtained from the NOGAPS model.

As additional data sources became available, AKDEMO SAR winds expanded to include ERS-2 and ALOS PALSAR imagery acquired through ASF and Envisat imagery acquired through the European Space Agency (ESA). Theoretical work during this period also expanded the capability for producing SAR winds to systems other than C-Band, prompted by the launches of Japan's ALOS (operating at L-band) and X-band imagery from both the German TerraSAR-X and the Italian COSMO-SkyMed satellites.

CURRENT OPERATIONS AT NOAA

One of the important results stemming from AKDEMO was the ability of SAR-derived winds to resolve the presence of fine-scale gap flow winds along the southern coast of Alaska (Loescher et al., 2006; Winstead et al., 2006; Figure 1). These winds, which can become intense over spatial scales of a few kilometers, represent a hazard to vessels and aircraft that makes them of particular interest to Alaska weather forecasters. Responding to a request from the National Weather Service (NWS) in 2008, the decision was made to transition the ANSWRS SAR-derived high-resolution wind products to operations within the NOAA NESDIS Office of Satellite and Product Operations (OSPO). The requested capabilities for SAR winds included the ability to produce SAR wind products at better than 1 km spatial resolution and with a wind speed accuracy of better

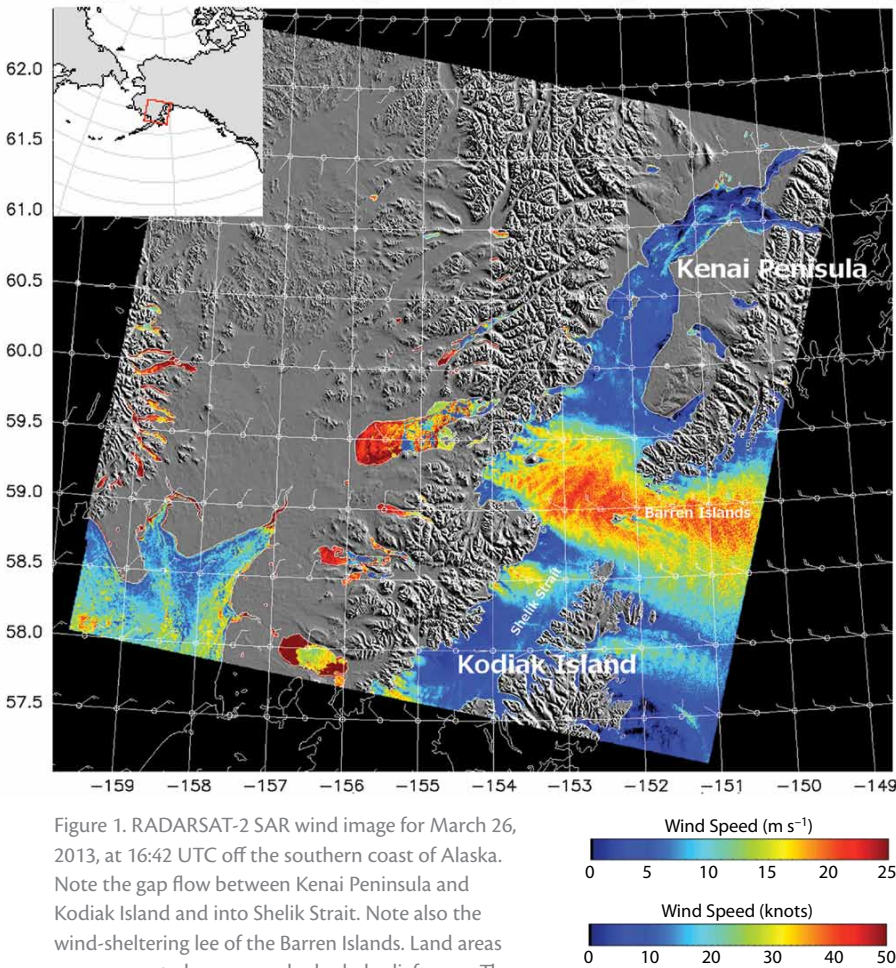


Figure 1. RADARSAT-2 SAR wind image for March 26, 2013, at 16:42 UTC off the southern coast of Alaska. Note the gap flow between Kenai Peninsula and Kodiak Island and into Shelik Strait. Note also the wind-sheltering lee of the Barren Islands. Land areas are represented as gray-scale shaded-relief maps. The inset map shows the location of the image off the southwestern portion of Alaska.

than 1 m s^{-1} for the range $3\text{--}15 \text{ m s}^{-1}$ (with reduced accuracy for winds from $16\text{--}50 \text{ m s}^{-1}$). The validated performance of better than 2 m s^{-1} (Monaldo et al., 2001) when compared against buoys and 1.3 m s^{-1} (Monaldo et al., 2004) when compared to QuikSCAT scatterometer measurements approaches these requirements, especially considering that buoys and scatterometers have their own inherent limitations. ANSWRS routinely processes winds at 500 m resolution.

In response to the NWS request, preliminary and critical system design reviews were held at NOAA in 2009. The architecture of the operational system involved substantial improvements from the one employed to support AKDEMO. The system was modularized to allow for ease in maintenance and upgrade and to allow for SAR winds products to be generated from multiple SAR scenes simultaneously. A front-end data ingester was put in place to convert the SAR data from each satellite data source into a standardized format in preparation for processing SAR winds. This conversion allows the system to be easily modified for future SAR satellites. Similarly, the winds processing produces a single, standardized netCDF output file from which other products (GeoTIFF, PNG, KMZ files) can be generated.

For the operational implementation, model wind directions are being obtained from the NOAA National Center for Climate Prediction (NCEP) Global Forecast System (GFS) model. The GFS model provides global winds on a 0.5° longitude-latitude grid four times a day (0, 6, 12, and 18Z), with forecasts at three-hour intervals out to seven days. The forecasts ensure the model wind direction availability for SAR winds

processing even if there is a temporary delay in model availability.

Figure 2 shows the data flow diagram for the NOAA system, with processes shown in blue and data files in gray. The system was declared operational on May 1, 2013, following six months of operational testing, completion of system documentation, and validation of SAR wind speed results. While the system can process SAR imagery from any of the SARs currently on orbit (see Table 1), the primary operational data source is RADARSAT-2. The system is being readied to accept imagery from ESA's Sentinel-1 system, expected to be launched in early 2014.

During the system development phase, the National Ice Center (NIC) requested that NOAA produce SAR-derived winds products from NIC's RADARSAT-2 imagery to support the center's ice analysts. The colored SAR wind imagery helps the NIC analysts to distinguish ice edge and extent

(Figure 3). Scattering from sea ice is substantially different from scattering over open water. Colors over ice should not be interpreted as wind speed. However, the different appearance of sea ice in wind speed imagery can make sea ice more conspicuous.

The availability of a near-real-time RADARSAT-2 data stream via the NIC provided an excellent opportunity for full end-to-end system testing and validation of the operational implementation of ANSWRS. Figure 4 shows validation results from comparing the SAR-derived winds to the GFS model. Attention was given to avoiding sea ice covered areas for the wind speed comparisons. Data were acquired at the NIC during the period from January 16 to February 28, 2013, UTC. SAR winds were averaged into $25 \text{ km} \times 25 \text{ km}$ areas for comparison with the model estimates. The error bars represent 95% confidence limits. The Ice Mapping System (IMS) ice mask (Helfrich et al.,

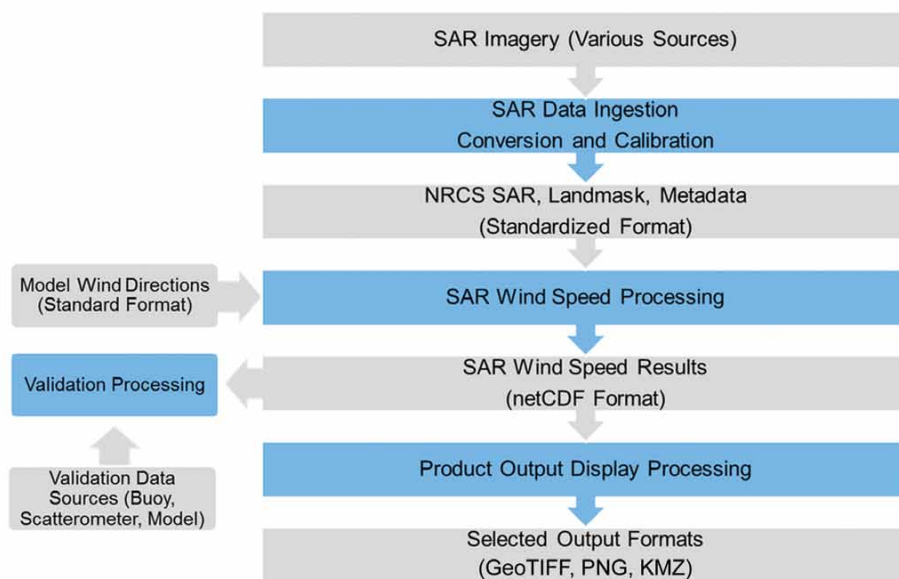


Figure 2. The processing flow for the NOAA high-resolution SAR winds operational product.

2007) produced by the NIC was used to exclude sea ice areas from the wind speed comparisons. The standard deviation of 2.1 m s^{-1} between the model and SAR wind speeds is quite good given that the model winds have a 1.8 m s^{-1} standard deviation with respect to buoy measurements (Yu and Gerald, 2004).

As mentioned earlier, there are a variety of C-band geophysical model functions that can be used to extract wind speeds from SAR imagery. Because these empirical model functions represent subtle differences in expected radar backscatter, they also partially compensate for slight calibration differences between

SAR instruments. For RADARSAT-2 SAR imagery at HH-polarization, validation testing found that the minimum differences and highest correlation between SAR wind speed retrievals and GFS model predictions occurred when using CMOD4 and $\alpha = 1.0$ in the polarization ratio function. Optimal wind retrieval results for RADARSAT-1 occurred when using CMOD4 and $\alpha = 0.6$. This is likely not due to scattering physics but rather to small differences in calibration between RADARSAT-1 and RADARSAT-2.

PROCESSING SEASAT DATA WITH ANSWRS

When Seasat was launched in 1978, the means to create SAR images from the raw signal were cumbersome and time-consuming. At first, signal film was processed on an optical bench to produce the imagery. Calibration to σ^0 was not considered feasible, and each time the original film was processed, the analog nature of the processing produced a slightly different image result. Within several years, some digital processors became available. Much of the early work by Beal et al. (1983) and Gerling (1986) on Seasat pass 1339 relied on

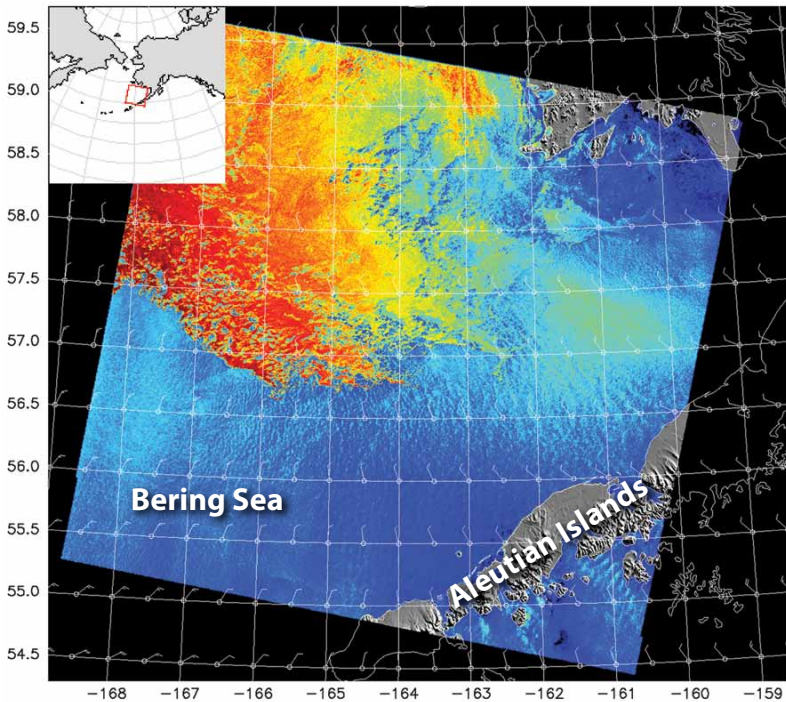


Figure 3. RADARSAT-2 SAR wind image acquired on March 18, 2013, 17:16 UTC, over the eastern Bering Sea. The image shows the difference in radar backscatter between water and sea ice. Land areas are represented as gray-scale shaded-relief maps. The inset map shows the location of the image off the southwestern portion of Alaska.

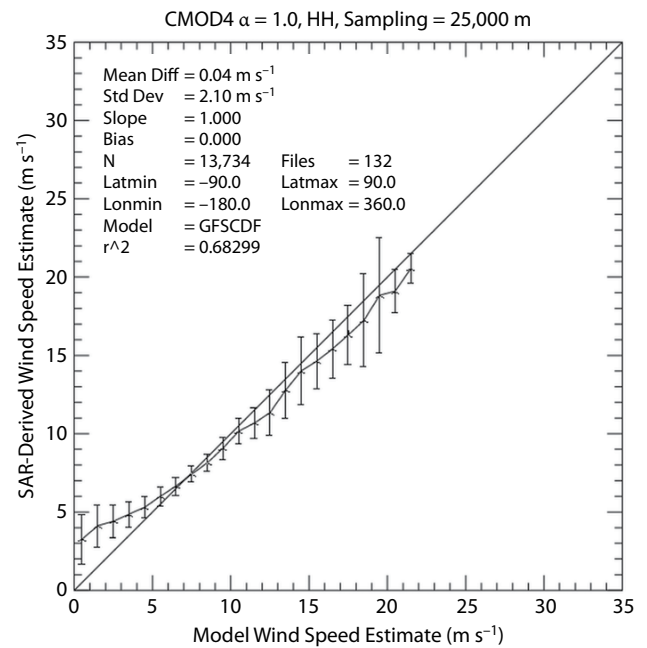
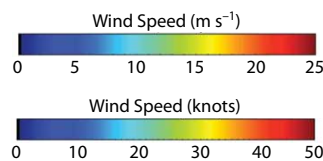


Figure 4. Comparison of RADARSAT-2 winds with Global Forecast System (GFS) model estimates.

new digitally processed images from MacDonald, Dettwiler and Associates Ltd. that were delivered on what was then considered a conventional medium for the transmission of digital data: 9-track tapes. A 6,250 bytes/in tape 2,400 feet (732 meters) long could hold roughly 180 Mbytes of data.

Given the existence of better digital SAR image processing capability, 35 years of experience in GMF development, and a radical increase in computing and storage ability, we thought it would be interesting to provide historical closure by determining the extent to which seminal Seasat pass 1339 could

again be used to produce a wind speed image. Seasat pass 1339 was digitally processed and graciously provided to us by the Alaska Satellite Facility to accomplish this.

ANSWRS has traditionally used numerical model wind direction estimates to initialize wind speed retrieval. Seasat is the only spaceborne SAR system to have had a co-located and simultaneous scatterometer wind vector measurement. With no model data easily available, we decided to use the 100 km resolution SASS retrievals to provide the necessary wind directions. Figure 5 is a plot of SASS wind vector retrievals

for a portion of pass 1339. Note that the swath is double-sided, though part of the left side retrievals for this pass were not valid. Nadir-to-spacecraft wind speed is provided, though no wind vector retrieval was possible.

Each SASS cell has four possible solutions. Figure 5 shows the solutions provided, color-coded as red, green, blue, and black. Gerling (1986) de-aliased these solutions by hand, using considerations of wind field continuity. We used his results to de-alias these SASS solutions to produce a set of wind directions equivalent to the GFS or NOGAPS model files that could be used for SAR

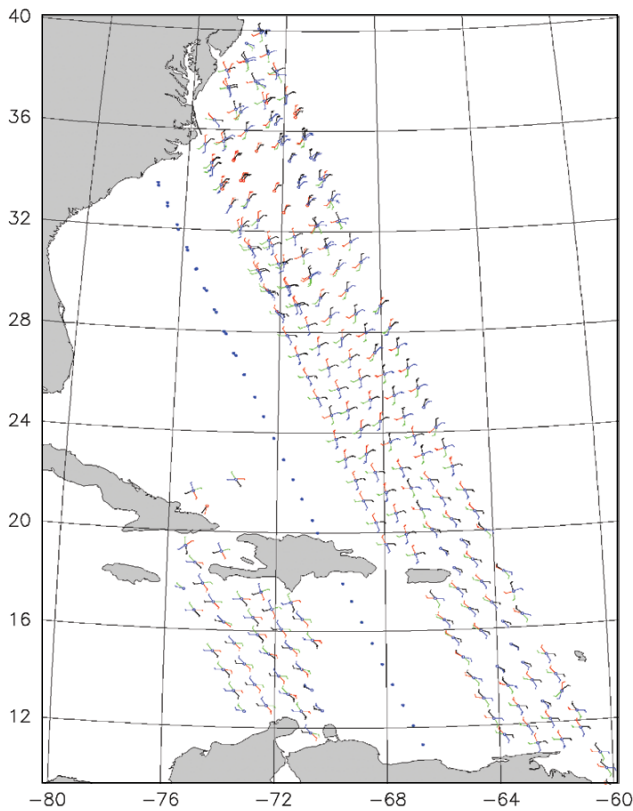


Figure 5. Seasat-A Scatterometer System (SASS) wind vectors from pass 1339. Wind vector solutions for each cell are shown as red, green, blue, and black wind barbs.

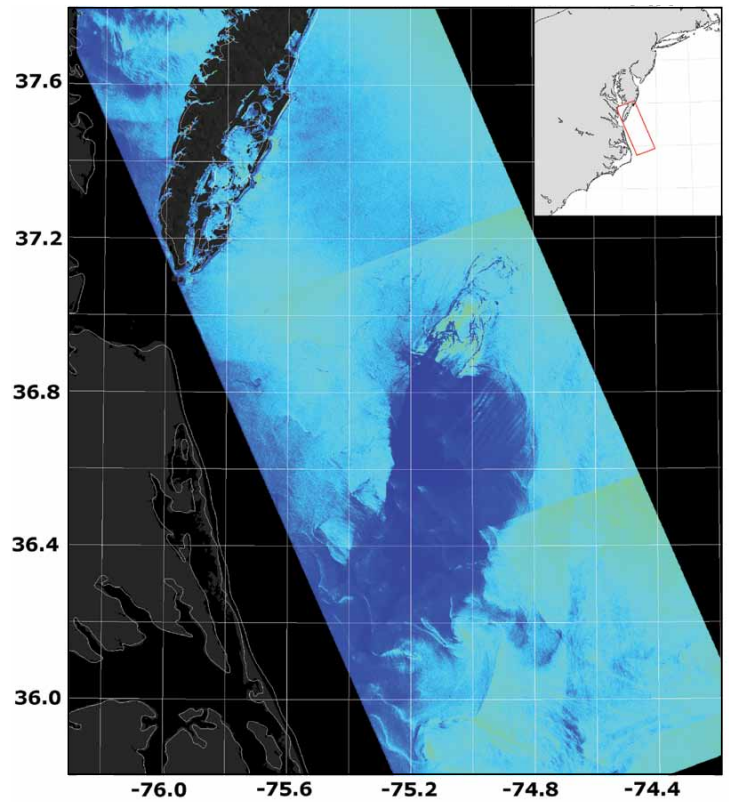
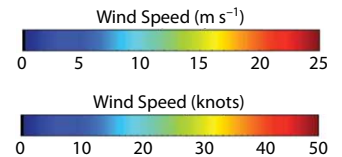


Figure 6. Seasat pass 1339 wind speed retrievals from the Johns Hopkins Applied Physics Laboratory/NOAA SAR Wind Retrieval System. The location of the pass is indicated by the map inset.



wind retrievals. Figure 6 is the resulting wind speed image from a portion of pass 1339 after application of the L-band GMF proposed by Isoguchi and Shimada (2009) and scaling of the measured NRCS values.

Because Seasat lasted only a few months (the full data set is comparatively modest in size), we might be able to combine wind direction data from SASS to make a systematic comparison of SAR retrieved and SASS wind speeds. This could act as a vicarious calibration of the Seasat SAR digital-processing output to NRCS.

THE FUTURE

With the availability of the newest X-band SAR systems (TerraSAR-X and COSMO-SkyMed), there has so far been only a modest effort in the development of an appropriate X-band geophysical model function. However, there is every reason to suspect that it is possible to compute X-band retrievals in a robust manner based on past work on scatterometers. Table 2 provides a reference listing of microwave frequency bands. Many conventional spaceborne scatterometers have traditionally operated at Ku-band. Other scatterometers and SAR winds have traditionally been retrieved using C-band. Because X-band lies between C-band and Ku-band, the

response of NRCS to wind speed and direction would be expected to lie somewhere between C-band and Ku-band.

Using data from TerraSAR-X, Thompson et al. (2012) attempted to define a GMF at X-band. They used two complementary approaches. The first was theoretical—a physics-based approach. They modeled the ocean surface spectrum (Elfouhaily et al., 1997; Romeiser et al., 1997) as a function of wind speed and direction and then computed the resulting backscatter power (at both VV- and HH-polarization). The second approach was empirical. Using well-validated model functions at C- and Ku-band, they interpolated a composite model function at both polarizations. Both results were evaluated against the high-resolution Weather Research and Forecasting (WRF) numerical forecast model (Skamarock et al., 2007) for reasonableness. Figure 7 is a sample wind speed image acquired off the coast of northern Germany.

For VV-polarization, the results of both approaches for the generation of an X-band GMF produced wind speeds consistent with the WRF model winds. The retrievals were also consistent with measurements made at nearshore locations. However, for HH-polarization, the theoretical model function systematically under-predicts σ^0 and, hence,

overestimates the retrieved wind speed.

The model functions constructed in the past for other frequency bands compared a large number of radar cross-section measurements with independent wind measurements. The initial work by Thompson et al. (2012) gives us an important head start in the right direction. As more and more X-band imagery becomes available, we are certain that a more complete and tuned X-band GMF model function will emerge.

Finally, further improvement in retrieval of C-Band based SAR-derived winds is expected with the anticipated launch of Sentinel-1A in early 2014, followed by Sentinel-1B, perhaps as early as 2016. In addition, Canada is currently planning to launch a three-spacecraft RADARSAT Constellation of C-band SARs in 2018. NOAA's operational SAR-derived wind product system is set up to handle the increased availability of SAR imagery from these systems.

CONCLUSION

In 1978, the United States launched Seasat with an onboard 25 m resolution, 100 km wide swath, L-band SAR designed to measure ocean surface wave spectra. The effects of variable ocean surface winds were clearly visible in the imagery, and preliminary attempts to compute wind speed were

Table 2. Summary of frequency bands used for wind retrieval.

Name	Frequency Range (GHz)	Wavelength Range (cm)
L	1–2	15–20
C	4–8	3.75–7.5
X	8–12	2.5–3.75
Ku	12–18	1.67–2.5

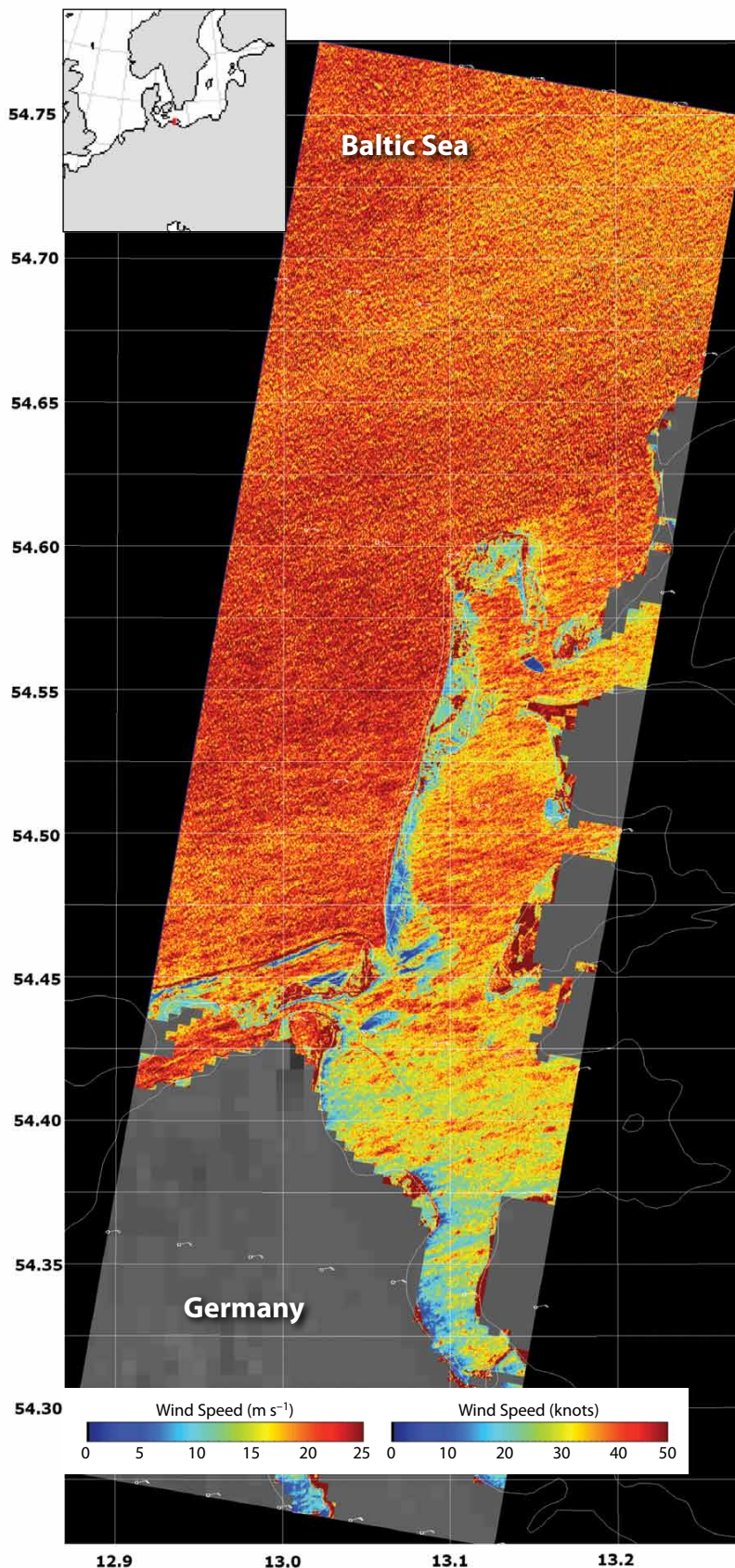


Figure 7. VV-polarization wind speed map from TerraSAR-X data acquired December 8, 2007, 05:24:38 UTC, off the northern coast of Germany as indicated by the map inset.

successful. Over the following 35 years, wind speed model functions, particularly at C-band, have matured and SAR imagery is more commonly available. NOAA/NESDIS has now implemented SAR wind speed retrievals as an operational product using primarily RADARSAT-2 data. With the upcoming Sentinel-1A/1B mission, RADARSAT Constellation, and the new generation of X-band SARs, we anticipate broad use of operational SAR winds.

ACKNOWLEDGEMENTS

The views, opinions, and findings contained here are those of the authors and should not be construed as an official NOAA or US government position, policy, or decision. 

REFERENCES

- Ager, T.P. 2013. An introduction to synthetic aperture radar imaging. *Oceanography* 26(2):20–33, <http://dx.doi.org/10.5670/oceanog.2013.28>.
- Attema, E.P.W. 1986. An experimental campaign for the determination of the radar signature of the ocean at C-band. Pp. 791–799 in *Proceedings of the Third International Colloquium on Spectral Signatures of Objects in Remote Sensing*. ESA SP-247, Les Arcs, France.
- Attema, E.P.W. 1991. The Active Microwave Instrument on-board the ERS-1 satellite. *Proceedings of the IEEE* 79:791–799, <http://dx.doi.org/10.1109/5.90158>.
- Beal, R.C. 1980. *The Seasat SAR Wind and Ocean Wave Monitoring Capabilities: A Case Study for Pass 1339m, 28 September 1978*. Technical Report S1R 79U-019, Johns Hopkins Applied Physics Lab, Laurel, MD, 15 pp.
- Beal, R.C., D.G. Tilley, and F.M. Monaldo. 1983. Large and small-scale spatial evolution of digitally processed ocean wave spectra from Seasat synthetic aperture radar. *Journal of Geophysical Research* 88:1,761–1,778, <http://dx.doi.org/10.1029/JC088iC03p01761>.
- Boggs, D.H. 1982. *Seasat Geophysical Data Record (GDR) Users Handbook: Scatterometer*. Technical Report D-129, Jet Propulsion Laboratory, California Institute of Technology, Pasadena, CA, 262 pp.
- Bragg, W.L. 1913. The diffraction of short electromagnetic waves by a crystal. *Proceedings of the Cambridge Philosophical Society* 17:43–57.

- Brown, R.A. 1980. Longitudinal instabilities and secondary flows in the planetary boundary layer: A review. *Reviews of Geophysics* 18:683–697, <http://dx.doi.org/10.1029/RG018i003p00683>.
- Brown, R.A. 1986. On a satellite scatterometer as an anemometer. *Journal of Geophysical Research* 91:2,221–2,232, <http://dx.doi.org/10.1029/JC088iC03p01663>.
- Elfouhaily, T., B. Chapron, K. Katsaros, and D. Vandemark. 1997. A unified directional spectrum for long and short wind-driven waves. *Journal of Geophysical Research* 102:15,781–15,796, <http://dx.doi.org/10.1029/97JC00467>.
- Fetterer, F., D. Gineris, and C.C. Wackerman. 1998. Validating a scatterometer wind algorithm for ERS-1 SAR. *IEEE Transactions on Geoscience and Remote Sensing* 36:479–492, <http://dx.doi.org/10.1109/36.662731>.
- Figa-Saldana, J., J.J.W. Wilson, E. Attema, R. Gelsthorpe, M.R. Drinkwater, and A. Stoffelen. 2002. The advanced scatterometer ASCAT on the meteorological operational (MetOp) platform: A follow on for European wind scatterometers. *Canadian Journal of Remote Sensing* 28:404–412, <http://dx.doi.org/10.5589/m02-035>.
- Fu, L.-L., and B. Holt. 1982. *Seasat Views Oceans and Seas with Synthetic Aperture Radar*. Technical Report JPL Publication 81–102, Jet Propulsion Laboratory, California Institute of Technology, Pasadena, CA. Available online at: <http://southport.jpl.nasa.gov/reports/seasat> (accessed August 4, 2013).
- Gerling, T.W. 1986. Structure of the surface wind field from the Seasat SAR. *Journal of Geophysical Research* 91:2,308–2,320, <http://dx.doi.org/10.1029/JC091iC02p02308>.
- Helfrich, S.R., D. McNamara, B.H. Ramsay, T. Baldwin, and T. Kasheta. 2007. Enhancements to, and forthcoming developments in the Interactive Multisensor Snow and Ice Mapping System (IMS). *Hydrological Processes* 21:1,576–1,586, <http://dx.doi.org/10.1002/hyp.6720>.
- Hersbach, H. 2003. CMOD5: An improved geophysical model function for ERS C-band scatterometry. Internal report, European Centre for Medium-Range Weather Forecast.
- Hersbach, H. 2008. CMOD5.N: A C-band geophysical model function for equivalent neutral wind. Internal Report 554, European Centre for Medium-Range Weather Forecast.
- Horstmann, J. 1997. Investigation of wind speed retrieval with synthetic aperture radar aboard the ERS-1/2 satellites. Technical Report GKSS 97/E/55, GKSS.
- Horstman, J., S. Falachetti, and S. Maresca. 2011. SAR wind speed retrieval with respect to tropical cyclones. International Ocean Vector Winds Science Team Meeting, Annapolis, MD.
- Horstmann, J., W. Kock, S. Lehner, and R. Tonboe. 2000. Wind retrieval over the ocean using synthetic aperture radar with C-band HH polarization. *IEEE Transactions on Geoscience and Remote Sensing* 38:2,122–2,131, <http://dx.doi.org/10.1109/36.868871>.
- Horstmann, J., W. Koch, S. Lehner, and R. Tonboe. 2002. Ocean winds from RADARSAT-1 ScanSAR. *Canadian Journal of Remote Sensing* 28:524–533, <http://dx.doi.org/10.5589/m02-043>.
- Horstmann, J., H. Schiller, J. Schultz-Stellenfelth, and S. Lehner. 2003. Global wind speed retrieval from SAR. *IEEE Transactions on Geoscience and Remote Sensing* 41:2,277–2,286, <http://dx.doi.org/10.1109/TGRS.2003.814658>.
- IFREMER. 1996. *Off-line Wind Scatterometer ERS Products: User Manual, Version 2.0*. C2-MUT-W-01-IF, IFREMER.
- Isoguchi, O., and M. Shimada. 2009. An L-Band ocean geophysical model function derived from PALSAR. *IEEE Transactions on Geoscience and Remote Sensing* 47:1,925–1,936, <http://dx.doi.org/10.1109/TGRS.2008.2010864>.
- Jones, W.L., V.E. Delnore, and E.M. Bracalente. 1981. Spaceborne Synthetic Aperture Radar for oceanography. Pp. 87–94 in *The Study of Mesoscale Winds*. The Johns Hopkins University Press, Baltimore, MD.
- Jordan, R.L. 1980. The Seasat: A synthetic aperture radar system. *IEEE Journal of Oceanic Engineering* 5:154–164, <http://dx.doi.org/10.1109/JOE.1980.1145451>.
- Kerr, D.E. 1951. *The Propagation of Short Radio Waves*. MIT Radiation Laboratory Series, vol. 13, McGraw-Hill, New York.
- Lehner, S., J. Horstmann, W. Koch, and W. Rosenthal. 1998. Mesoscale wind measurements using recalibrated ERS SAR images. *Journal of Geophysical Research* 103:7,847–7,856, <http://dx.doi.org/10.1029/97JC02726>.
- Loescher, K.A., G.S. Young, B.A. Coller, and N.S. Winstead. 2006. Climatology of barrier jets along the Alaskan coast. Part I: Spatial and temporal distributions. *Monthly Weather Review* 124:437–453, <http://dx.doi.org/10.1175/MWR3037.1>.
- Monaldo, F., V. Kerbaol, and the SAR Wind Team. 2003. The SAR measurement of ocean surface winds: An overview. In *Proceedings of the Second Workshop on Coastal and Marine Applications of SAR*. European Space Agency, Svalbard, Norway. Available online at: http://earth.esa.int/workshops/cmasar_2003/papers/E02mona.pdf (accessed August 2, 2013).
- Monaldo, F.M., D.R. Thompson, R.C. Beal, W.G. Pichel, and P. Clemente-Colón. 2001. Comparison of SAR-derived wind speed with model predictions and buoy comparisons. *IEEE Transactions on Geoscience and Remote Sensing* 39:2,587–2,600, <http://dx.doi.org/10.1109/36.974994>.
- Monaldo, F.M., D.R. Thompson, W.G. Pichel, and P. Clemente-Colón. 2004. A systematic comparison of QuikSCAT and SAR ocean surface wind speeds. *IEEE Transactions on Geoscience and Remote Sensing* 42:283–291, <http://dx.doi.org/10.1109/TGRS.2003.817213>.
- Moore, R.K. 1974. Simultaneous active and passive microwave response of the earth: The Skylab RADSCAT experiment. Pp. 189–217 in *Proceedings of the Ninth International Symposium on Remote Sensing of the Environment, vol. I*. University of Michigan, Ann Arbor, MI.
- Moreira, A., P. Prats-Iraola, M. Younis, G. Kriger, I. Hajnski, and K.P. Papathanassiou. 2013. A tutorial on synthetic aperture radar. *IEEE Geoscience and Remote Sensing Magazine* 1:6–43, <http://dx.doi.org/10.1109/MGRS.2013.2248301>.
- Naderi, F.M., M.H. Freilich, and D.G. Long. 1991. Spaceborne radar measurement of wind velocity over the ocean: An overview of the NSCAT scatterometer system. *Proceedings of the IEEE* 79:850–866, <http://dx.doi.org/10.1109/5.90163>.
- Phillips, O.M. 1988. Radar returns from the sea surface: Bragg scattering and breaking waves. *Journal of Physical Oceanography* 18:1,065–1,074, [http://dx.doi.org/10.1175/1520-0485\(1988\)018<1065:RRFTSS>2.0.CO;2](http://dx.doi.org/10.1175/1520-0485(1988)018<1065:RRFTSS>2.0.CO;2).
- Pichel, W.G., and P. Clemente-Colón. 2000. NOAA CoastWatch SAR applications and demonstration. *The Johns Hopkins University Technical Digest* 21:49–57.
- Plant, W.J. 1990. Bragg scattering of electromagnetic waves from the air/sea interface. Pp. 41–108 in *Surface Waves and Fluxes*, vol. II. G.L. Geernaert and W.J. Plant, eds, Kluwer Academic Publishers.
- Rice, S.O. 1951. Reflection of electromagnetic waves from slightly rough surfaces. *Communications on Pure and Applied Mathematics* 4:351–378.
- Romeiser, R., W. Alpers, and V. Wissemann. 1997. An improved composite model for the radar backscattering cross section of the ocean surface: Part 1. Theory and model validation/optimization by scatterometer data. *Journal of Geophysical Research* 102:25,237–25,250, <http://dx.doi.org/10.1029/97JC00190>.
- Skamarock, W.C., J.B. Klemp, J. Dudhia, D.O. Gill, W. Wang, and J.G. Powers. 2007. A description of the Advanced Research WRF version 2. Technical Report, NCAR Technical Note NCAR/TN-468+STR, Mesoscale and Microscale Meteorological Division, National Center for Atmospheric Research, Boulder,

- CO. Available online at: http://www.mmm.ucar.edu/wrf/users/docs/arw_v2.pdf (accessed August 2, 2013).
- Spencer, M.W., C. Wu, and D.G. Long. 1997. Tradeoffs in the design of a spaceborne scanning pencil-beam scatterometer: Application to SeaWinds. *IEEE Transactions on Geoscience and Remote Sensing* 35:115–126, <http://dx.doi.org/10.1109/36.551940>.
- Stoffelen, A., and D.L.T. Anderson. 1993. Wind retrieval and ERS-1 scatterometer radar backscatter measurements. *Advances in Space Research* 13:53–60, [http://dx.doi.org/10.1016/0273-1177\(93\)90527-1](http://dx.doi.org/10.1016/0273-1177(93)90527-1).
- Stoffelen, A., and D. Anderson. 1997a. Scatterometer data interpretation: Measurement and inversion. *Journal of Atmospheric and Oceanic Technology* 14:1,298–1,313, [http://dx.doi.org/10.1175/1520-0426\(1997\)014<1298:SDIMSA>2.0.CO;2](http://dx.doi.org/10.1175/1520-0426(1997)014<1298:SDIMSA>2.0.CO;2).
- Stoffelen, A., and D. Anderson. 1997b. Scatterometer data interpretation: Estimation and validation of the transfer function: CMOD4. *Journal of Geophysical Research* 102(C3):5,767–5,780, <http://dx.doi.org/10.1029/96JC02860>.
- Thompson, D.R., and R.C. Beal. 2000. Mapping high-resolution wind fields using synthetic aperture radar. *The Johns Hopkins University Technical Digest* 21:58–67.
- Thompson, D.R., T.M. Elfouhaily, and B. Chapron. 1999. Polarization ratio for microwave backscattering from the ocean surface at low to moderate incidence angles. Pp. 1,671–1,673 in *Proceedings of the 1998 IEEE International Geoscience and Remote Sensing Symposium*, vol. 3. IGARSS '98, <http://dx.doi.org/10.1109/IGARSS.1998.692411>.
- Thompson, D.R., J. Horstmann, A. Mouche, N.S. Winstead, R. Sterner, and F.M. Monaldo. 2012. Comparison of high-resolution wind fields extracted from TerraSAR-X SAR imagery with predictions from the WRF mesoscale model. *Journal of Geophysical Research* 117, C02035, <http://dx.doi.org/10.1029/2011JC007526>.
- Thompson, D.R., F.M. Monaldo, N.S. Winstead, W.G. Pichel, and P. Clemente-Colón. 2001. Combined estimates improve high-resolution coastal wind mapping. *Eos, Transactions, American Geophysical Union* 82:368–374, <http://dx.doi.org/10.1029/01EO00278>.
- Vachon, P.W., and F.W. Dobson. 1996. Validation of wind vector retrieval from ERS-1 SAR images over the ocean. *The Global Atmosphere-Ocean System* 5:177–187.
- Valenzuela, G.R. 1968. Scattering of electromagnetic waves from a tilted slightly rough surface. *Radio Science* 3:1,057–1,066.
- Vesecky, J.F., and R.H. Stewart. 1982. The observation of ocean surface phenomena using imagery from the SEASAT synthetic aperture radar. *Journal of Geophysical Research* 87:3,397–3,430, <http://dx.doi.org/10.1029/JC087iC05p03397>.
- Wackerman, C.C. 2000. Estimating wind vectors from RADARSAT synthetic aperture radar imagery. Technical Report 10032100-1-T, Veridian ERIM International, Ann Arbor, MI.
- Wackerman, C.C., W.G. Pichel, and P. Clemente-Colón. 2003. Automated estimation of wind vectors from SAR. Paper presented at the 12th Conference on Interactions of the Sea and Atmosphere, 83rd AMS Annual Meeting, Long Beach, CA. Abstract available online at: https://ams.confex.com/ams/annual2003/techprogram/paper_58270.htm (accessed August 2, 2013).
- Wackerman, C.C., R. Rufenach, R.A. Shuchman, J.A. Johannessen, and K.L. Davidson. 1996. Wind vector retrieval using ERS-1 synthetic aperture radar imagery. *IEEE Transactions on Geoscience and Remote Sensing* 34:1,343–1,352, <http://dx.doi.org/10.1109/36.544558>.
- Weissman, D.E., D. King, and T.W. Thompson. 1979. Relationship between hurricane surface winds and L-band radar backscatter from the sea surface. *Journal of Applied Meteorology* 18:1,023–1,034, [http://dx.doi.org/10.1175/1520-0450\(1979\)018<1023:RBHWSA>2.0.CO;2](http://dx.doi.org/10.1175/1520-0450(1979)018<1023:RBHWSA>2.0.CO;2).
- Winstead, N.S., B. Colle, N. Bond, G. Young, J. Olson, K. Loescher, F. Monaldo, D. Thompson, and William Pichel. 2006. Using SAR remote sensing, field observations, and models to better understand coastal flows in the Gulf of Alaska. *Bulletin of the American Meteorological Society* 87:788–800, <http://dx.doi.org/10.1175/BAMS-87-6-787>.
- Wright, J.W. 1966. Backscattering from capillary waves with application to sea clutter. *IEEE Transactions on Antennas and Propagation* 14:749–754, <http://dx.doi.org/10.1109/TAP.1966.1138799>.
- Wright, J.W. 1968. A new model for sea clutter. *IEEE Transactions on Antennas and Propagation* 16:217–223, <http://dx.doi.org/10.1109/TAP.1968.1139147>.
- Yu. T.-W., and V.M. Gerald. 2004. Evaluation of NCEP operational model forecasts of surface wind and pressures fields over the oceans. Paper presented at the 16th Conference on Numerical Weather Prediction, Seattle, WA, January 2004. Abstract available online at: https://ams.confex.com/ams/84Annual/techprogram/paper_68792.htm (accessed August 2, 2013).